

A WENO Algorithm for the Radiative Transfer and Ionized Sphere at Reionization

Jing-Mei Qiu ^a, Chi-Wang Shu ^a, Long-Long Feng ^{b,c},
Li-Zhi Fang ^d

^a*Division of Applied Mathematics, Brown University, Providence, RI 02912, USA*

^b*Purple Mountain Observatory, Nanjing, 210008, P.R. China*

^c*National Astronomical Observatories, Chinese Academy of Science, Chao-Yang District, Beijing 100012, P.R. China*

^d*Department of Physics, University of Arizona, Tucson, AZ 85721, USA*

Abstract

We show that the algorithm based on the weighted essentially nonoscillatory (WENO) scheme with anti-diffusive flux corrections can be used as a solver of the radiative transfer equations. This algorithm is highly stable and robust for solving problems with both discontinuities and smooth solution structures. We test this code with the ionized sphere around point sources. It shows that the WENO scheme can reveal the discontinuity of the radiative or ionizing fronts as well as the evolution of photon frequency spectrum with high accuracy on coarse meshes and for a very wide parameter space. This method would be useful to study the details of the ionized patch given by individual source in the epoch of reionization. We demonstrate this method by calculating the evolution of the ionized sphere around point sources in physical and frequency spaces. It shows that the profile of the fraction of neutral hydrogen and the ionized radius are sensitively dependent on the intensity of the source.

Key words: cosmology: theory, gravitation, hydrodynamics, methods: numerical, shock waves

PACS: 95.30.Jx, 07.05.Tp, 98.80.-k

1 Introduction

In the study of cosmic large scale structures formation, one generally focuses on the inhomogeneity of the density and velocity fields of dark matter and

baryon gas, but assumes that the distribution of background radiation is uniform. This would be a reasonable approximation when the universe is transparent. Therefore, the effect of radiative transfer is generally ignored in the study of large scale structures on low redshift. However, the fluctuations in the radiation field is essential in understanding the early universe, especially in the epoches around reionization. Radiative transfer problems are no longer to be overlooked. Many numerical solvers for the radiative transfer equation have been proposed (Abel et al. 1999, Ciardi et al. 2001, Gnedin & Abel 2001, Sokasian et al. 2001, Razoumov et al. 2002, Cen 2002, Maselli et al. 2003).

In this paper, we will introduce the algorithm of the radiative transfer equations based on the finite difference weighted essentially non-oscillatory (WENO) scheme (Jiang & Shu 1996) modified with anti-diffusive flux corrections (Xu & Shu 2005). It has been shown that the Boltzmann equations can be solved by this WENO method with reasonable computational speed at least for one or two spatial dimensions and two or three phase space dimensions plus time (Carrillo et al. 2003, 2006). The WENO code is effective to capture discontinuities as well as to resolve complicated flow features. Moreover, it is also significantly superior over piecewise smooth solutions containing discontinuities. It has advantages over the Monte-Carlo codes in eliminating fluctuations, in obtaining accurate probability density functions, and in accurately resolving time transients of the system. Considering the equation of radiative transfer basically is the same as the Boltzmann equation, the WENO algorithm for the radiative transfer is straightforward. Moreover, a hybrid algorithm of hydrodynamic/N-body simulation based on WENO scheme has been successfully developed (Feng et al. 2004). This result also motivated us to extend the WENO scheme to radiative transfer problems. It would be a necessary preparation to develop solver of hydrodynamic/radiative transfer problems.

We will demonstrate the WENO algorithm by applying the WENO code to the Strömgren sphere. The structure and evolution of an individual Strömgren sphere are important for the understanding of the reionization process. The ionization of baryon gas surrounding high redshift objects, such as quasars, stars of first generation, generally is modelled by the Strömgren sphere (Madau & Rees, 2000; Cen & Haiman 2000; White et al. 2003; Stuart et al. 2004; Yu & Lu 2005). The Strömgren sphere usually is described as a fully ionized region, sharply divided from the neutral hydrogen region on the outside of the sphere. Therefore, we should require the algorithm to be able to 1.) capture the sharp boundary between the ionized and neutral regions, and their time-dependence; 2.) accurately calculate the small amount of neutral hydrogen in the sphere and ionized hydrogen outside the sphere. These two points can be realized by the the WENO numerical scheme, as it is effective for problems containing both strong discontinuities and smooth flow structures.

The paper is organized as follows. Section 2 describes the WENO numerical

scheme. Section 3 gives the numerical solutions of the Strömgren sphere. The discussion and conclusion are presented in §4. The derivation of the equation of the radiative transfer is given in the Appendix.

2 Numerical solver of the WENO scheme

The radiative transfer equation in an expanding universe is (see the Appendix)

$$\frac{\partial J}{\partial(ct)} + \frac{\partial}{\partial x^i} \left(\frac{n^i}{a} J \right) + \frac{\partial}{\partial \omega} (HJ) = -(k_\nu + 3H)J + S, \quad (1)$$

where $J(t, \mathbf{x}, \nu, n_i)$ is the specific intensity, a the cosmic factor, $H = \dot{a}/a$, ν the frequency of photon, $\omega \equiv \ln 1/\nu$, and n_i a unit vector in the direction of photon propagation. k_ν and S are, respectively, the absorption and sources of photons.

To demonstrate the WENO method, we consider the simplest case. We ignore the expansion of the universe. This approximation is correct if the time scale of evolution of photon distribution is much less than the time scale of cosmic expansion. Moreover, the physical and phase spaces are assumed to be 1-dimensional with coordinate r . In this case, the radiative transfer equation is

$$\frac{\partial J}{\partial ct} + \frac{\partial J}{\partial r} = -k_\nu J + S \quad (2)$$

The computational domain is discretized into a tensor product mesh. The mesh is taken to be uniform in the r -direction, and to be smooth non-uniform in the ν -direction, i.e.

$$\begin{aligned} r_i &= i\Delta r; & i &= 0, 1, 2, \dots, N_r, \\ \nu_j &= 2^{\xi_j}; & j &= 0, 1, 2, \dots, N_\nu, \end{aligned} \quad (3)$$

where $\Delta r = r_{\max}/N_r$ is the mesh size in the r -direction, and $\xi_j = j\Delta\xi$, $\Delta\xi = \log_2 \nu_{\max}/N_\nu$ is the transformed mesh size in the ν direction. r_{\max} and ν_{\max} are, respectively, the sizes of the numerical domain, which are adjusted in the numerical experiment such that $J(t, r, \nu) \simeq 0$, for $r > r_{\max}$ and all t and ν , and $J(t, r, \nu) \simeq 0$, for $\nu > \nu_{\max}$ and all t and r .

The approximations to the point values of the solution $J(t^n, r_i, \nu_j)$, denoted by $J_{i,j}^n$, are obtained with an approximation to the spacial derivatives using the 5th order finite difference WENO method (Jiang & Shu 1996) with anti-diffusive flux corrections (Xu & Shu 2005).

- Approximation to the derivatives:

To calculate $\partial J / \partial r$, the variable ν is fixed and the approximation is performed along the r -line

$$\frac{\partial}{\partial r} J(t^n, r_i, \nu_j) \approx \frac{1}{\Delta r} (\hat{h}_{i+1/2}^a - \hat{h}_{i-1/2}^a)$$

where the numerical flux $\hat{h}_{i+1/2}^a$ is obtained with the procedure given below. We can use the upwind fluxes without flux splitting in the fifth order WENO approximation because the wind direction is fixed (positive). To obtain the sharp resolution of the contact discontinuities, the anti-diffusive flux corrections are used in our code.

First, we denote

$$h_i = J(t^n, r_i, \nu_j), i = -2, -1, \dots, N_r + 2$$

where n and j are fixed. The numerical flux from the regular WENO procedure is obtained by

$$\hat{h}_{i+1/2}^- = \omega_1 \hat{h}_{i+1/2}^{(1)} + \omega_2 \hat{h}_{i+1/2}^{(2)} + \omega_3 \hat{h}_{i+1/2}^{(3)}$$

where $\hat{h}_{i+1/2}^{(m)}$ are the three third order fluxes on three different stencils given by

$$\begin{aligned} \hat{h}_{i+1/2}^{(1)} &= \frac{1}{3} h_{i-2} - \frac{7}{6} h_{i-1} + \frac{11}{6} h_i, \\ \hat{h}_{i+1/2}^{(2)} &= -\frac{1}{6} h_{i-1} + \frac{5}{6} h_i + \frac{1}{3} h_{i+1}, \\ \hat{h}_{i+1/2}^{(3)} &= \frac{1}{3} h_i + \frac{5}{6} h_{i+1} - \frac{1}{6} h_{i+2}, \end{aligned}$$

and the nonlinear weights ω_m are given by

$$\omega_m = \frac{\tilde{\omega}_m}{\sum_{l=1}^3 \tilde{\omega}_l}, \quad \tilde{\omega}_l = \frac{\gamma_l}{(\varepsilon + \beta_l)^2},$$

with the linear weights γ_l given by

$$\gamma_1 = \frac{1}{10}, \quad \gamma_2 = \frac{3}{5}, \quad \gamma_3 = \frac{3}{10},$$

and the smoothness indicators β_l given by

$$\begin{aligned} \beta_1 &= \frac{13}{12} (h_{i-2} - 2h_{i-1} + h_i)^2 + \frac{1}{4} (h_{i-2} - 4h_{i-1} + 3h_i)^2 \\ \beta_2 &= \frac{13}{12} (h_{i-1} - 2h_i + h_{i+1})^2 + \frac{1}{4} (h_{i-1} - h_{i+1})^2 \\ \beta_3 &= \frac{13}{12} (h_i - 2h_{i+1} + h_{i+2})^2 + \frac{1}{4} (3h_i - 4h_{i+1} + h_{i+2})^2. \end{aligned}$$

ε is a parameter to avoid the denominator to become 0 and is taken as $\varepsilon = 10^{-5}$ times the maximum magnitude of the initial condition J in the computation of this paper. The reconstruction of the finite difference WENO flux on the downwind side $\hat{h}_{i+1/2}^+$ is obtained in a mirror symmetric fashion with respect to $x_{i+1/2}$ as that for $\hat{h}_{i+1/2}^-$.

The anti-diffusive flux corrections are based on the fluxes obtained from the regular WENO procedure. It is given by

$$\hat{h}_{i+1/2}^a = \hat{h}_{i+1/2}^- + \phi_i \text{minmod} \left(\frac{h_i - h_{i-1}}{\eta} + \hat{h}_{i-1/2}^- - \hat{h}_{i+1/2}^-, \hat{h}_{i+1/2}^+ - \hat{h}_{i+1/2}^- \right), \quad (4)$$

where $\eta = \Delta t / \Delta r$ is the cfl number and the minmod function is defined as

$$\text{minmod}(a, b) = \begin{cases} 0, & \text{if } ab \leq 0 \\ a, & \text{if } ab > 0, |a| \leq |b| \\ b, & \text{if } ab > 0, |b| < |a|. \end{cases} \quad (5)$$

ϕ_i of eq.(4) is the discontinuity indicator between 0 and 1, defined as

$$\phi_i = \frac{\beta_i}{\beta_i + \gamma_i},$$

where

$$\beta_i = \left(\frac{\alpha_i}{\alpha_{i-1}} + \frac{\alpha_{i+1}}{\alpha_{i+2}} \right)^2, \quad \gamma_i = \frac{|u_{\max} - u_{\min}|^2}{\alpha_i}, \quad \alpha_i = (|h_{i-1} - h_i| + \zeta)^2,$$

with ζ being a small positive number taken as 10^{-6} in our computation. u_{\max} and u_{\min} are the maximum and minimum values of h_i for all grid points. With the definition above, we will have $0 \leq \phi_i \leq 1$. $\phi_i = O(\Delta r^2)$ in the smooth regions and ϕ_i is close to 1 near strong discontinuities. The purpose of the anti-diffusive flux corrections is to improve the resolution of contact discontinuities without sacrificing accuracy and stability of the original WENO scheme.

- Approximation to the evolution with time

The time-derivative $\partial/\partial t$ in each step Δt is calculated by the third order TVD Runge-Kutta method as

$$\begin{aligned} J^{(1)} &= J^n + \Delta t L(J^n, t^n) \\ J^{(2)} &= J^n + \frac{1}{4} \Delta t L(J^n) + \frac{1}{4} \Delta t L(J^{(1)}) \\ J^{n+1} &= J^n + \frac{1}{6} \Delta t L(J^n) + \frac{1}{6} \Delta t L(J^{(1)}) + \frac{2}{3} \Delta t L(J^{(2)}) \end{aligned}$$

where L is the approximation to the spatial derivatives and the source terms:

$$L(J) \approx -\frac{\partial}{\partial r} J - k_\nu J + S$$

The Runge-Kutta method needs to be modified considering the modification on the anti-diffusive flux \hat{f}^a by

$$\begin{aligned} J^{(1)} &= J^n + \Delta t L(J^n, t^n) \\ J^{(2)} &= J^n + \frac{1}{4} \Delta t L'(J^n) + \frac{1}{4} \Delta t L(J^{(1)}) \\ J^{n+1} &= J^n + \frac{1}{6} \Delta t L''(J^n) + \frac{1}{6} \Delta t L(J^{(1)}) + \frac{2}{3} \Delta t L(J^{(2)}) \end{aligned}$$

where the operator L is defined by the anti-diffusive flux \hat{h}^a given by eq.(4), and the operator L' is defined by the modified anti-diffusive flux \bar{h}^a as

$$\bar{h}_{i+1/2}^a = \begin{cases} \hat{h}_{i+1/2}^- + \min\left(\frac{4(h_i - h_{i-1})}{\eta}, \right. \\ \quad \left. + \hat{h}_{i-1/2}^- - \hat{h}_{i+1/2}^-, \hat{h}_{i+1/2}^+ - \hat{h}_{i+1/2}^- \right), \\ \quad \text{if } bc > 0, |b| < |c|, \\ \hat{h}_{i+1/2}^a, & \text{otherwise} \end{cases} \quad (6)$$

and L'' is defined by the modified anti-diffusive flux \tilde{h}^a ,

$$\tilde{h}_{i+1/2}^a = \begin{cases} \hat{h}_{i+1/2}^- + \min\left(\frac{6(h_i - h_{i-1})}{\eta}, \right. \\ \quad \left. + \hat{h}_{i-1/2}^- - \hat{h}_{i+1/2}^-, \hat{h}_{i+1/2}^+ - \hat{h}_{i+1/2}^- \right), \\ \quad \text{if } bc > 0, |b| < |c|, \\ \hat{h}_{i+1/2}^a, & \text{otherwise} \end{cases} \quad (7)$$

Here $b = (h_i - h_{i-1})/\eta + \hat{h}_{i-1/2}^- - \hat{h}_{i+1/2}^-$, $c = \hat{h}_{i+1/2}^+ - \hat{h}_{i+1/2}^-$.

We have given the details of the WENO algorithm with anti-diffusive flux corrections only for the one dimensional case to save space. The finite difference WENO scheme is ideally suited for multi-dimensional calculations, as derivatives in each direction can be approximated in an one dimensional setting by fixing the other variables, while still maintaining high order accuracy and stability. We refer to (Carrillo et al. 2003, 2006) for more details of WENO approximations to Boltzmann equations. Our radiative transfer equations [Eq.(1)] are of the same form as the Boltzmann equations in (Carrillo et al. 2003, 2006) and hence the algorithms developed there can be applied here without difficulty.

3 Ionized sphere

3.1 Ionized source in a uniform medium

As a test, we consider a point photon source located at the center $\mathbf{x} = 0$ of a uniformly distributed medium. Assuming the source is monochromatic with frequency ν_0 , and all photons are emitted along the radial direction, we have

$$S(t, \mathbf{x}, \nu, \mathbf{n}) = f(t, \mathbf{x})\delta(\nu - \nu_0)\delta(\mathbf{n} - \mathbf{e}_r). \quad (8)$$

and

$$f(t, \mathbf{x}) = \begin{cases} E/V, & \text{at the center } \mathbf{x} = 0 \\ 0, & \text{otherwise,} \end{cases} \quad (9)$$

where E is the total energy of photons emitted from the sources per unit time. When $V \rightarrow 0$, $f(t, \mathbf{x}) \rightarrow E\delta(\mathbf{x})$.

In this case, Eq.(1) could be written in the spherical coordinates as

$$\frac{\partial J}{\partial(ct)} + \frac{1}{r^2} \frac{\partial}{\partial r} (r^2 n^r J) = -kJ, \quad r \neq 0 \quad (10)$$

where the absorption coefficient k is given by $k = n\sigma$, n being the number density of particle of the medium, and σ the absorption cross-section. In this problem, both n and σ are assumed to be constants.

We define $r^2 J \equiv J'(t, r)\delta(\nu - \nu_0)\delta(\mathbf{n} - \mathbf{e}_r)$. Then eq.(10) becomes

$$\frac{\partial J'}{\partial(ct)} + \frac{\partial}{\partial r} J' = -kJ', \quad r \neq 0. \quad (11)$$

For simplicity, we drop the prime, and use $J(t, r)$ for $J'(t, r)$ below. It will not cause confusion between the J in eqs.(11) and (10), as the former is a function of t, r , while the later is a function of t, r, ν and n_i . The source term gives a boundary condition at $r = 0$ as

$$\lim_{r \rightarrow 0} 4\pi J(t, r) = E \quad (12)$$

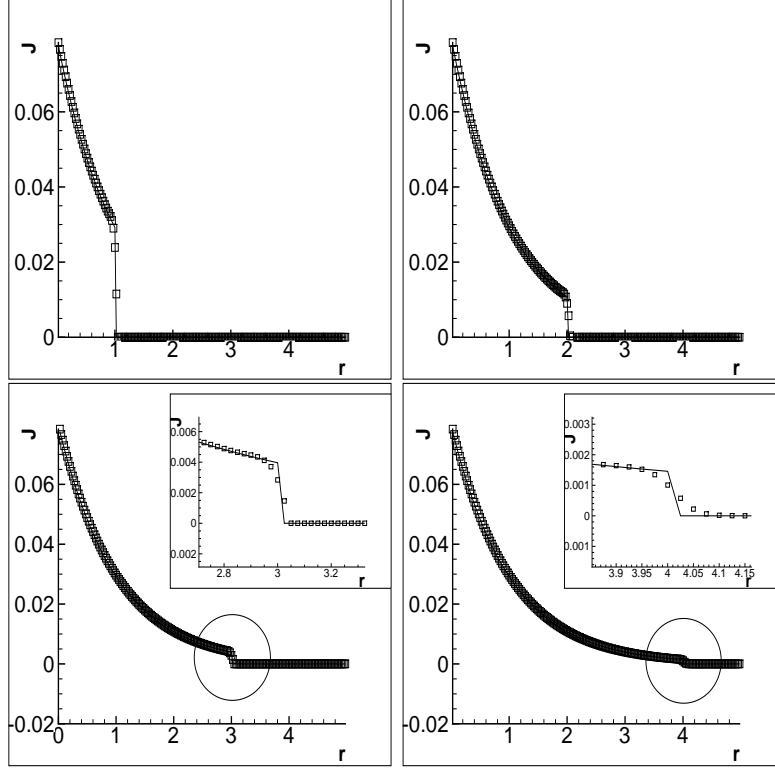


Fig. 1. The curves of $J(t, r)$ given by the numerical solution at $N_r = 200$ (square) and the exact solution (solid line). $J(t=0, r)=\frac{1}{4\pi}$. The time is taken to be $t = 1.0$ (top left); $t = 2.0$ (top right); $t = 3.0$ (bottom left) and $t = 4.0$ (bottom right). The small windows in the bottom figures are the zoom-in version of the corresponding regions in the circles.

Assuming the source starts to emit photon at $t = 0$, the initial condition is then

$$J(t = 0, r) = \begin{cases} E/4\pi, & r = 0 \\ 0, & r > 0. \end{cases} \quad (13)$$

Subject to the conditions (12) and (13), the exact solution of eq.(11) is

$$J(t, r) = \theta(t - r) \frac{E}{4\pi} e^{-kr}, \quad (14)$$

where $\theta(x)$ is a step function: $\theta(x) = 1$, if $x \geq 0$; and $\theta(x) = 0$, if $x < 0$. The step function is from the radiative front, which propagates with the speed of light $r = t$.

Eq.(11) has the same shape as Eq.(2). Similarly, we can apply the WENO scheme to solve Eq.(11). The boundary condition eq.(12) makes us to take the

inflow condition at $r = 0$ as

$$J(t^n, r_i) = E/4\pi, \quad \text{for} \quad i = 0, -1, -2.$$

The boundary condition at $r = r_{\max}$ is:

$$J_{N_r+i,j} = J_{N_r-1,j}, \quad \text{for} \quad i = 0, 1, 2$$

Figure 1 plots both the numerical solution and exact solution at time $t = 1.0, 2.0, 3.0, 4.0$. Clearly, the numerical result displays an excellent agreement with the exact solution even when the number N_r is only 200. The discontinuity at the radiative front $r = t$ is also well reproduced in the WENO scheme.

3.2 The profile of an ionized sphere

We now consider a realistic problem: the ionization of a uniformly distributed hydrogen gas with number density n by a point UV photon source located at $r = 0$. This problem is the well known Strömberg sphere if the profile of the ionized sphere is approximated by two sharply divided regions as

$$f_{\text{HI}}(r) \simeq \begin{cases} 0 & \text{if } r < R_s \\ 1 & \text{if } r > R_s \end{cases} \quad (15)$$

where $f_{\text{HI}} \equiv n_{\text{HI}}/n$, $n_{\text{HI}}(t, \mathbf{x})$ is the number density of neutral hydrogen, HI. Eq.(15) means that within the sphere of radius R_s around the source, hydrogen is fully ionized, while outside the sphere hydrogen atoms remain neutral. R_s is called the ionized radius of the Strömberg sphere, which can be determined by the balance between the rate of recombinations and the emission \dot{N} of ionizing photons (Strömberg 1939, Spitzer 1978, Osterbrook 1989)

$$R_s = \left(\frac{3\dot{N}}{4\pi\alpha_{\text{HII}}n^2} \right)^{1/3}, \quad (16)$$

where α_{HII} is the hydrogen recombination coefficient.

The sharp profile eq.(15), and then eq.(16), are reasonable if the mean free path of photon $\lambda \simeq 1/\sigma_0 n$ is much less than R_s . For strong sources, like quasars $\dot{N} \simeq 10^{57} \text{ s}^{-1}$, R_s is much larger than λ . However, for weak sources, like population III stars $\dot{N} \leq 10^{50}$, λ is comparable, or even larger than R_s . In this case, the profile eq.(15) is no longer valid. Even for strong sources, we need to study the small deviation of the profile of ionized sphere from

eq.(15). The profile should be found by solving the radiative transfer equation with proper boundary and initial conditions. Moreover, the profile eq.(15) describes the final state of the ionized sphere around a strong source. To study the reionization history of the universe, we may need the information of the formation of the ionized sphere i.e. the time-dependence of $f_{\text{HII}}(t, r)$. This also requires to solve the radiative transfer equation.

To calculate the profile of the ionized sphere, we can still use eq.(11), boundary condition eq.(12), and initial condition eq.(13). The absorption coefficient now is given by

$$k_{\nu_0} = \sigma(\nu_0)n_{\text{HI}}(t, \mathbf{x}) \quad (17)$$

where $\sigma(\nu_0)$ is the absorption cross section at the ionization frequency ν_0 . We have $\sigma_0 = \sigma(\nu_0) = 6.3 \times 10^{-18} \text{ cm}^2$.

The number density of neutral hydrogen $n_{\text{HI}}(t, \mathbf{x})$ is determined by the ionization equilibrium equation

$$\frac{df_{\text{HI}}}{dt} = \alpha_{\text{HII}}n_e f_{\text{HII}} - \Gamma_{\gamma\text{HI}}f_{\text{HI}} - \Gamma_{\text{eHI}}n_e f_{\text{HI}}. \quad (18)$$

where $f_{\text{HI}}(t, r) \equiv n_{\text{HI}}/n$, $f_{\text{HII}}(t, r) \equiv n_{\text{HII}}/n$. We will assume electron density $n_e = n_{\text{HII}}$. This means that the electrons from ionized helium are ignored. The photoionization is given by

$$\Gamma_{\gamma\text{HI}} = \frac{1}{r^2} \frac{J(t, r)}{h\nu_0} \sigma_0. \quad (19)$$

The parameters α_{HII} and Γ_{eHI} are the recombination coefficient and collision ionization, respectively, which can be found in e.g. Theuns et al (1998).

Let us rescale the variables by $t' = c\sigma(\nu_0)nt$, $r' = \sigma(\nu_0)nr$. It means that t' and r' are, respectively, the time and distance in the units of mean free flight time and mean free path, $1/\sigma_0(\nu_0)n$, of photon $h\nu_0$ in neutral hydrogen gas with density n . In the Λ CDM model, $n = 1.88 \times 10^{-7}(1+z_r)^3 \text{ cm}^{-3}$, where z_r is the redshift of reionization, the unit of t' is $0.89 \times 10^6(1+z_r)^{-3} \text{ years}$, and the unit of r' is $0.27(1+z_r)^{-3} \text{ Mpc}$. We also rescale the intensity by $J'' = J(\sigma^2 n / ch\nu_0)$. Eqs.(11) can then be rewritten as

$$\frac{\partial J''}{\partial t'} + \frac{\partial J''}{\partial r'} = -f_{\text{HI}}J'', \quad r \neq 0 \quad (20)$$

The boundary condition (12) and initial condition (13) are, respectively

$$J''(t, r = 0) = J''_0 \quad (21)$$

$$J''(t = 0, r) = \begin{cases} 0, & \text{if } r > 0 \\ J''_0, & \text{if } r = 0 \end{cases} \quad (22)$$

With this rescaling, the photoionization term of eq.(19) is $\Gamma_{\gamma\text{HI}}/n = (J''/r'^2)(cn\sigma_0)$. The intensity of source is $\dot{N} = 4\pi J(0)/h\nu = 5.05 \times 10^{52} J''_0(1 + z_r)^{-3} \text{ s}^{-1}$.

3.2.1 Strong sources

For strong sources, R_s is much larger than the mean free path. We can replace the rate equation (18) by ionization equilibrium equation $df_{\text{HI}}/dt = 0$, or $\alpha_{\text{HII}}f_{\text{HI}}^2 - (\Gamma_{\gamma\text{HI}}/n + 2\alpha_{\text{HII}})f_{\text{HI}} + \alpha_{\text{HII}} = 0$, where the small term $\Gamma_{e\text{HI}}$ is also dropped. A typical numerical result of the $f_{\text{HI}}(t, r)$ profile is shown in Figure 2, in which $J''_0 = 4.2$, or $\dot{N} = 2.16 \times 10^{53}(1 + z_r)^{-3}$. The calculation is performed with $N_r = 1000$.

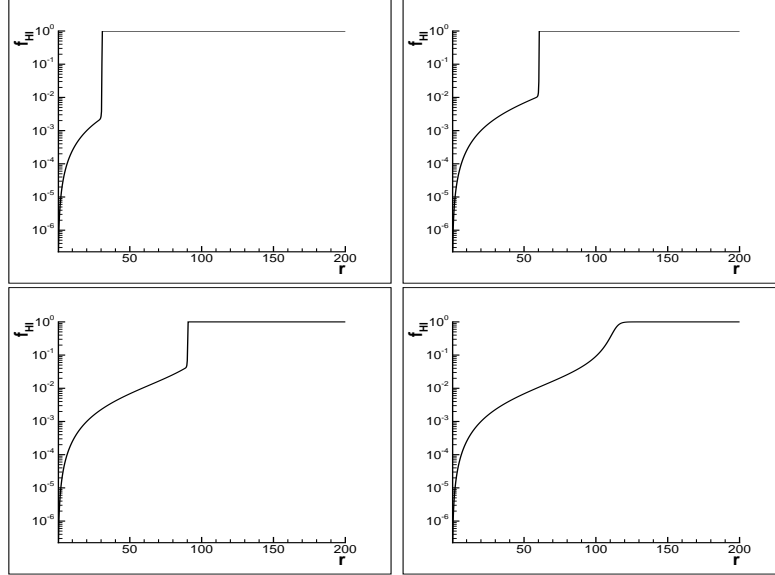


Fig. 2. $f_{\text{HI}}(t, r)$ vs. r at time $t = 30.0$ (top left), 60.0 (top right), 90.0 (bottom left), 140.0 (bottom right) for a strong source $J''_0 = 4.2$, or $\dot{N} = 2.16 \times 10^{53}(1 + z_r)^{-3} \text{ s}^{-1}$. The parameter N_r of the numerical calculation is taken to be 1000. The ionized radius $R_s=122.04$.

Figure 2 shows that the code can well reveal the jump at radiative front $r = t$, which propagates with the speed of light. The evolution of the ionized range

can approximately be described as

$$f_{\text{HI}}(t, r) \simeq \begin{cases} \theta(r - t), & t \leq t_s \\ \theta(r - t_s), & t > t_s \end{cases} \quad (23)$$

When t is small, the increase of ionized sphere is following the radiative front $r = t$. The increase will be halted, when the ionization equilibrium is totally established, and the ionized sphere becomes time-independent. For the case of $J''(0) = 4.2$, the final state arrives at $t_s \simeq 1.22 \times 10^2$. Since the bottom right panel of Figure 2 is for $t = 140 > t_s$, it should be the final state of the ionized sphere. The profile of the final state can be approximately described by the Strömgren sphere profile eq.(15), and ionized radius R_s is about 122 mean free path.

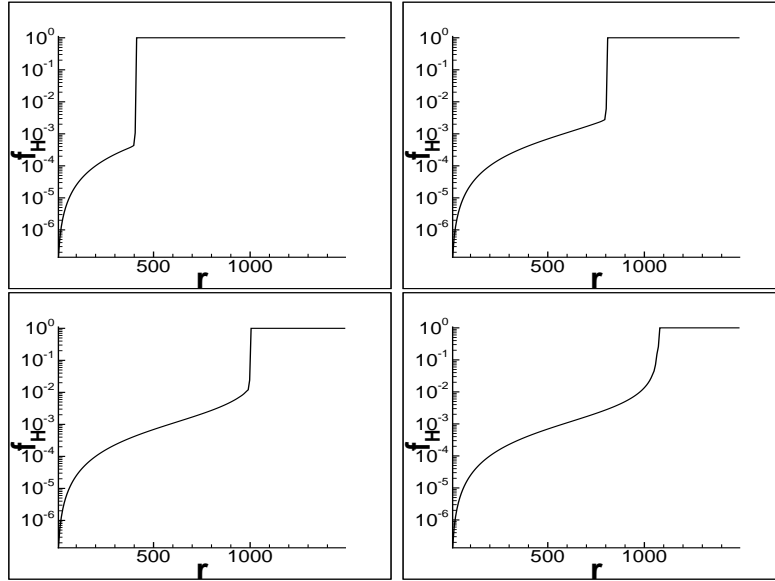


Fig. 3. $f_{\text{HI}}(t, r)$ vs. r at time $t = 400.0$ (top left), 800.0 (top right), 1000.0 (bottom left), 1100.0 (bottom right) for a strong source $J_0'' = 4.2 \times 10^3$ or $\dot{N} = 2.6 \times 10^{56}(1 + z_r)^{-3} \text{ s}^{-1}$. The parameter N_r of the numerical calculation is taken to be 200. The ionized radius $R_s=1080.0$.

If we define an effective ionized radius $r_{\text{HII}}(t)$ by

$$\frac{1}{3}r_{\text{HII}}^3(t) = \int_0^{r=t} f_{\text{HII}}(r, t)r^2 dr, \quad (24)$$

we have $r_{\text{HII}}(t) \simeq t$ when $t < t_s$. The physical meaning of r_{HII} is clear. It gives an equivalent sphere, within which hydrogen is fully ionized. The ionized radius is essentially the same as the radiative front. Therefore, for strong sources, the radiative front and ionized radius are the same in all time $t < t_s$.

From Figure 2 we can also see that the neutral hydrogen fraction within the ionized sphere $r < t_s$ actually is not exactly equal to zero. Although the profile (15) may still be reasonable, f_{HI} can be as large as 10^{-2} near the ionized radius. We also calculated the profile with very strong source like $J_0'' = 4.2 \times 10^3$, which is shown in Figure 3. In this case the source intensity J_0'' is larger than that of Figure 2 by a factor of 10^3 , and therefore, the radius of R_s of Figure 3 is larger than that of 2 by a factor of 10. There is also neutral hydrogen left behind the ionization front. These small amounts of HI are stable, i.e. independent of the parameter N_r . The neutral hydrogen remained in the ionized sphere is not always negligible.

3.2.2 Weak Sources

If the Strömgren sphere radius R_s of a source is comparable or less than the mean free path, it is a weak source. In this case, we should use eq.(18) to describe the ionization evolution. In the range of r less than the mean free path, i.e. $r' \ll 1$, the photoionization Γ_{HI} is large. We can keep only the photoionization term $\Gamma_{\text{HI}} f_{\text{HI}}$ on the r.h.s. of eq.(18).

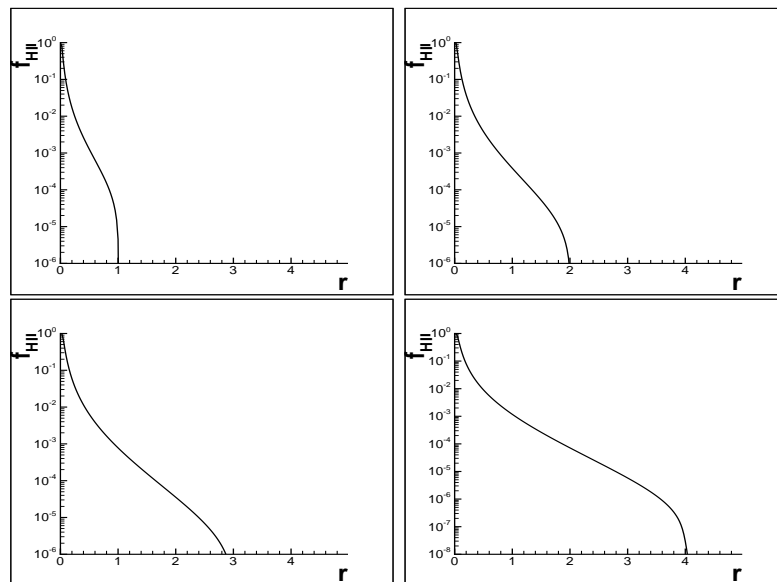


Fig. 4. $f_{\text{HII}}(t, r)$ vs. r at time $t = 1.0$ (top left), 2.0 (top right), 3.0 (bottom left), 4.0 (bottom right) for a weak source $J_0'' = 0.001$ or $\dot{N} = 5.05 \times 10^{49} (1 + z_r)^{-3}$. The parameter N_r of the numerical calculation is taken to be 200.

A solution numerical solution of the profile $f_{\text{HII}}(t, r) = 1 - f_{\text{HI}}(t, r)$ at $t=1, 2, 3$, and 4 are shown in Figure 4, in which the source intensity is $J_0'' = 0.001$ or $\dot{N} = 5.05 \times 10^{49} (1 + z_r)^{-3} \text{ s}^{-1}$. The calculation is performed with $N_r = 200$.

We can see from Fig. 4 that the profile is very different from strong source. The spatial range of $f_{\text{HI}}(t, r)$ significantly less than 1 (or $f_{\text{HII}}(t, r)$ significantly larger than zero) is much less than t , because the total number of photons

emitted from sources within time t is less than the number of atoms within radius $r = t$. $f_{\text{HI}}(t, r)$ is gradually increasing with r . Although the non-zero range of the ionized fraction $f_{\text{HII}} = 1 - f_{\text{HI}}(t, r)$ increases with time, the range $f_{\text{HI}}(t, r) > 10^{-2}$ is always small. It implies that the ionized sphere probably is not transparent to Ly α photons.

Figure 4 shows that the effective ionized radius $r_{\text{HII}}(t)$ [eq.(24)] for weak sources is $r_{\text{HII}}(t) < t$, or $r_{\text{HII}}(t)/t < 1$. The growth of the ionized range is much slower than the radiative front. With the increase of source intensity, $r_{\text{HII}}(t)/t$ will gradually approach to 1, and then, the solution will transfer to the case of strong sources.

3.3 Evolution of the frequency spectrum

Let us consider a point source emitting photons with a power law frequency spectrum. The source function S is then

$$S(t, \mathbf{x}, \nu, \mathbf{n}) = \begin{cases} (E(\nu)/V)\delta(\mathbf{n} - \mathbf{e}_{\mathbf{r}}), & \text{at center} \\ 0, & \text{otherwise,} \end{cases} \quad (25)$$

where $E(\nu) = E(\nu/\nu_0)^{-\alpha}$, α is the index of the power law. Therefore, different from the problems of §3.1 and 3.2, we should consider the variable ν of the frequency space, i.e. J is a function of t , r , and ν . The equation of J is still the same as eq.(11), but the absorption coefficient is ν -dependent

$$k_\nu = \sigma(\nu)n_{\text{HI}}(t, \mathbf{x}),$$

where the cross section $\sigma(\nu) = 6.3 \times 10^{-18}(\nu_0/\nu)^3 \text{ cm}^2$. The boundary condition now should be

$$\lim_{r \rightarrow 0} J(t, r, \nu) = J_0(\nu/\nu_0)^{-\alpha} \quad (26)$$

and the initial condition is

$$J(t = 0, r, \nu) = J_0(\nu/\nu_0)^{-\alpha}\theta(r = 0) \quad (27)$$

We still rescale the variables by $t' = cn\sigma(\nu_0)t$, $r' = n\sigma(\nu_0)r$, $\nu' = \nu/\nu_0$ and $J'' = Jn\sigma^2(\nu_0)/ch$. Then eq. (19) is updated as follow,

$$\frac{\partial J''}{\partial t'} + \frac{\partial J''}{\partial r'} = - \left(\frac{1}{\nu'}\right)^3 f_{\text{HI}} J'' \quad (28)$$

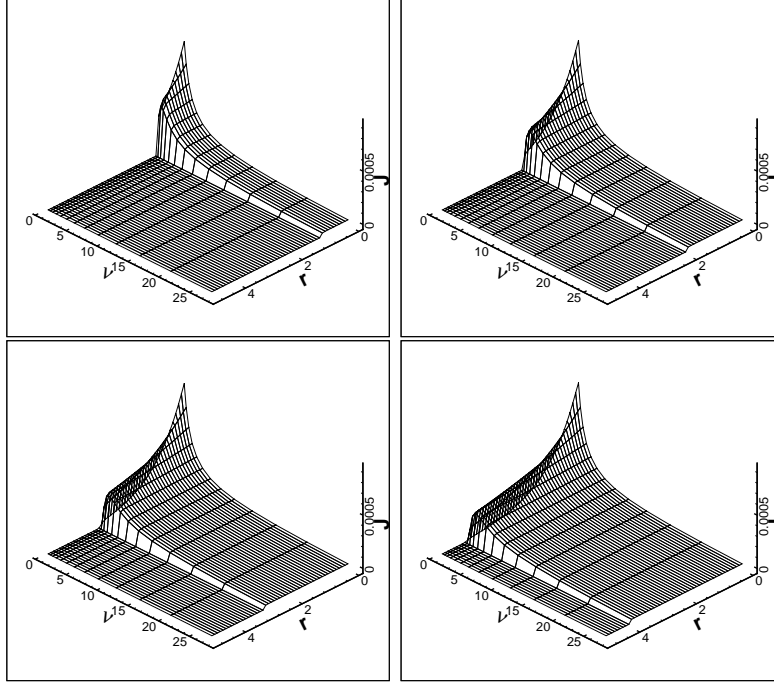


Fig. 5. A numerical result of the intensity $J''(t, r, \nu)$ for $J_0'' = 0.001$ at time $t = 1.0$ (top left), 2.0 (top right), 3.0 (bottom left), and 4.0 (bottom right). The mesh is taken to be $N_r=100$, $N_\nu=100$, and $\nu_{\max}=10^6$.

If we ignore the ionizing heating, f_{HI} or $n_{\text{HI}}(t, \mathbf{x})$ is still determined by eq.(18), but $\Gamma_{\gamma\text{HI}}(t, \mathbf{x})$ should be given by

$$\Gamma_{\gamma\text{HI}}(t, \mathbf{x}) = \frac{1}{r^2} \int_{\nu_0}^{\infty} d\nu \frac{J(t, r, \nu)}{h\nu} \sigma(\nu). \quad (29)$$

This integration could be worked out with a quadrature formula accurate of order 4

$$\int_{\nu_0}^{\infty} f(x) dx = \Delta x \sum_{j=j_0}^{\infty} w_j f(j\Delta x) + O(\Delta x^4) \quad (30)$$

where $\nu_0 = j_0 \Delta x$, and the weights w_j are given by

$$w_{j_0} = \frac{3}{8}, \quad w_{j_0+1} = \frac{7}{6}, \quad w_{j_0+2} = \frac{23}{24},$$

and

$$w_{j_0+j} = 1, \quad \text{for } j > 2.$$

By having a non-uniform mesh in the ν -direction, one cannot use this quadrature formula directly. However, since a uniform mesh size is used on ξ , with

$\nu_j = 2^{\xi_j}$, we can perform the numerical integration with respect to ξ using (29).

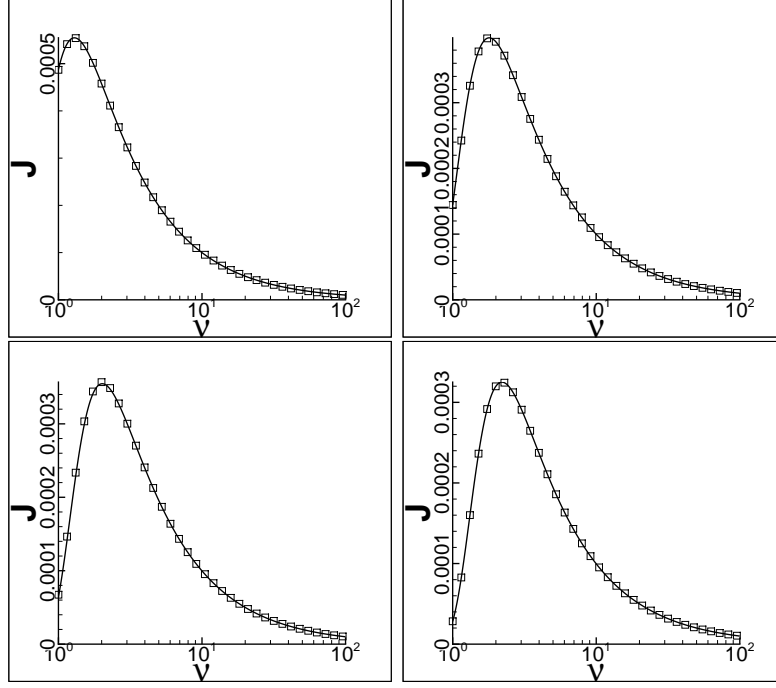


Fig. 6. A numerical solution of J vs. $\log \nu$ with $N_r = 100$, $N_\nu = 100$ (square) and the reference solution (solid) obtained with $N_r = 1000$, $N_\nu = 1000$, at time $t = 4.0$ and $r=0.8$ (top left), $r=2.0$ (top right), $r=2.8$ (bottom left) and $r=3.6$ (bottom right).

A numerical result of $J''(t, r, \nu)$ for $J''_0 = 10^{-3}$ and $\alpha = 1$ is shown in Figure 5, which is obtained by the mesh $N_x=100$, $N_\nu=100$ and $\nu_{\max}=10^6$. It displays the evolution of the frequency-dependence of J'' . We notice that for the high frequency $\nu > 50$, the intensity J'' is almost independent of t and r , while the frequency spectrum at $\nu < 10$ is significantly dependent on both t and r .

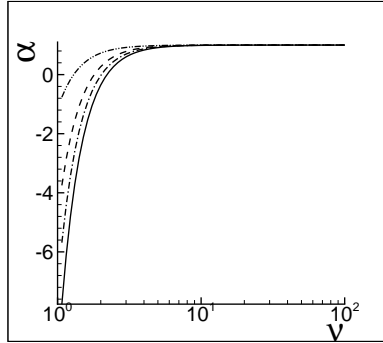


Fig. 7. α vs. $\log \nu$ of the numerical solution with $N_r = 100$, $N_\nu = 100$ at time $t=4.0$ and $r=0.8$ (dash dot dot line), $r=2.0$ (dash line), $r=2.8$ (dash dot line) and $r = 3.6$ (solid line).

The evolution of the frequency spectrum can be seen more clearly in Figure 6, which shows J vs. ν at time $t = 4.0$ and position $r = 0.8, 2.0, 2.8$ and

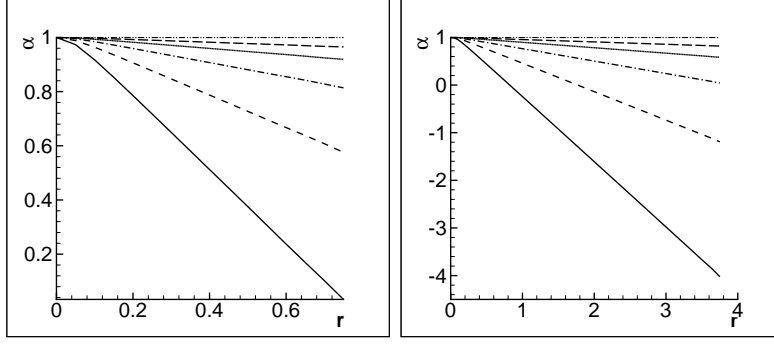


Fig. 8. α vs. r with samples of $N_r = 100$, $N_\nu = 100$ at time $t = 1.0$ (left) and 4.0 (right) for wave bands $\nu = 1.32$ (solid line), $\nu = 1.74$ (dash line), $\nu = 2.29$ (dash dot line), $\nu = 3.02$ (dot line), $\nu = 3.98$ (long dash line) and $\nu = 63.10$ (dash dot dot line).

3.6. The results of Figure 6 given by $N_r = 100$ and $N_\nu = 100$ are the same as that obtained with $N_r = 1000$ and $N_\nu = 1000$. Therefore, the algorithm is also stable and highly accurate in the frequency space. From Figure 6, we can see a significant r -dependence of the spectrum. At small r , the spectrum essentially is of power law, while at $r = 3.6$ it is similar to a spectrum of self-absorption, i.e. it is low at $\nu \simeq 1$, and shows a peak at $\nu \simeq 2$.

Generally, self-absorption leads to the lack of photons with $\nu \simeq 1$, and therefore, to the hardening of the frequency spectrum of photons. One can measure the hardening by the index of power law defined by

$$\alpha = -\frac{\partial \ln J}{\partial \ln \nu}. \quad (31)$$

Figure 7 plots α vs. ν at different positions r and shows that α becomes smaller at $\nu < 10$. Figure 8 gives α vs. r for several ν . It shows that α becomes smaller at larger r .

4 Concluding remarks

We described a numerical solver for radiative transfer problems based on the WENO scheme modified with anti-diffusive flux corrections. It has high order of accuracy and good convergence, and is also highly stable and robust for solving problems with both discontinuities and smooth solution structures. Using the Strömgren sphere or ionized sphere as numerical tests, we showed that this code is able to resolve the sharp ionized front under a wide parameter range, such as intensity of the source \dot{N} varying from $10^{49} - 10^{57}(1 + z_r)^{-3} \text{ s}^{-1}$, which covers various sources responsible for the early reionization in the universe.

Since the WENO scheme needs more floating point operations per cell than those of the PPM and TVD schemes, it leads to twice or more loss of computational speed. Nevertheless, it has been already successfully applied to kinetic equations of distribution function in phase space with one or two spatial dimensions and two or three phase space dimensions. It can provide the solution of evolution in both the physical space as well as the frequency space. Therefore, the WENO scheme would be useful to study the early stage of reionization, in which ionized region is generally an isolated patch given by individual source with various configuration.

We demonstrate this algorithm with the problems of spherical ionized region exposed to a point source. It is shown that the radial profile of the fraction of ionized hydrogen is sensitively dependent on the intensity of the sources. Although for strong sources the Strömgren sphere provides a good approximation to the ionized sphere, the profile of the sphere actually can not always be approximated as fully ionized spheres sharply separated with neutral hydrogen region. Even for strong sources, the neutral hydrogen remained in the Strömgren ionized sphere may still be significant and important. There are 1-D radiative transfer codes, such as CLOUDY94 (e.g. Maselli et al. 2003), which are capable of capturing the sharp boundary of the Strömgren sphere. However, they yield large errors of the neutral hydrogen remained in the sphere. Our result shows that the WENO codes can effectively handle the uncertainty around discontinuities.

We studied the time-dependence of the ionized radius $r_{\text{HII}}(t)$. We found that for strong sources, $r_{\text{HII}}(t) \simeq t$ when $r_{\text{HII}} < R_s$. This is similar to the result of Madau & Rees 2000. For weak sources, we have $r_{\text{HII}}(t) < t$. However, the evolution of $r_{\text{HII}}(t)$ can not be fitted by $r_{\text{HII}}(t) \propto t^{1/3}$, which will yields unphysical result $dr_{\text{HII}}(t)/dt > 1$ at small t (e.g. Cen & Haiman 2000; Yu & Lu 2005). Moreover, the WENO algorithm provides also the solution of the evolution of the photon's frequency spectrum of an ionized sphere.

The WENO scheme for radiative transfer problems could be incorporated with the Euler hydrodynamics. For instance, it is straightforward to generalize the calculation of a Strömgren sphere to take account of the hydrodynamic effects of the hydrogen gas sphere even when the gaseous sphere undergoes shocks.

Acknowledgments

This work is supported in part by the US NSF under the grants AST-0506734 and AST-0507340. LLF acknowledges support from the National Science Foundation of China under the grant 10573036.

A Radiative transfer equations

Considering a universe described by a Robertson-Walker metric, we have

$$ds^2 = g_{\mu\nu}dx^\mu dx^\nu = dt^2 - a^2(t)g_{ij}x^i x^j, \quad (\text{A.1})$$

where we take $c = 1$. The summation is over 0 to 3 for repeated Greek indices, 0 to 3 for Latin indices, $a(t)$ is the cosmic factor and $g_{ij} = \delta_{ij} - h_{ij}$. We consider below the flat universe, i.e. $h_{ij} = 0$. The distribution function $f(t, x^i, p^\alpha)$ of photons is defined by

$$dN = -f(x^\alpha, p^\alpha) 2\delta^D(p^\alpha p_\alpha) d\mathcal{V}_x d\mathcal{V}_p, \quad (\text{A.2})$$

where dN is the number of photons in the invariant phase space volume element of

$$d\mathcal{V}_x = a^3 p^0 dx^1 dx^2 dx^3 \quad d\mathcal{V}_p = dp_0 dp_1 dp_2 dp_3. \quad (\text{A.3})$$

The variables x^i is comoving coordinate, $p^0 = dt/d\lambda$, and $p^i = a(t)dx^i/d\lambda$ are 4 momentum, λ being the affine parameter. The Dirac-delta function $\delta^D(p^\alpha p_\alpha)$ in eq.(A.2) is due to the 4 momentum p^α of photons to be null, i.e. $p_\alpha p^\alpha = 0$.

The Boltzmann equation of the distribution function $f(x^\alpha, p^\alpha)$ is given by (e.g. Bernstein 1988)

$$\frac{\partial f}{\partial t} + \frac{dx^i}{dt} \frac{\partial f}{\partial x^i} - \frac{\dot{a}}{a} p^i \frac{\partial f}{\partial p^i} = Q, \quad (\text{A.4})$$

where Q is collision term, of which the variables are also t, x^i, ν, n^i . Define $n^i = a(dx^i/dt)$, it is a unit vector in the direction of photon propagation, $\mathbf{n} \cdot \mathbf{n} = 1$. With n^i , we have $p^i = p^0 n^i$, or $p^0 = \hbar\nu/c$, the frequency ν of photon. From eq.(A.4), the equation of the distribution function $f(t, x^i, \nu, n^i)$ is

$$\frac{\partial f}{\partial t} + \frac{1}{a} \frac{\partial}{\partial x^i} (n^i f) - H\nu \frac{\partial f}{\partial \nu} = Q, \quad (\text{A.5})$$

where the Hubble constant $H = \dot{a}/a$. From the definition eq.(A.2) of f , the specific intensity $J \propto \nu^3 f$, which is also a function of t, \mathbf{x}, ν and n^i . Moreover, if Q is mainly given by absorption and emission sources, Eq.(A.5) yields the equation of specific intensity as follows

$$\frac{\partial J}{\partial t} + \frac{1}{a} \frac{\partial}{\partial x^i} (n^i J) - H \left(\nu \frac{\partial J}{\partial \nu} - 3J \right) = -k_\nu J + S. \quad (\text{A.6})$$

where k_ν is the absorption coefficient, and S the source function. Eq.(A.6) is the equation of radiative transfer in the universe. The equation (A.6) can be rewritten as in the format of a conservation flux as

$$\frac{\partial J}{\partial t} + \frac{\partial}{\partial x^i} \left(\frac{n^i}{a} J \right) + \frac{\partial}{\partial \omega} (H J) = -(k_\nu + 3H)J + S, \quad (\text{A.7})$$

where $\omega \equiv \ln 1/\nu$. Therefore, it can be solved by the WENO scheme.

References

- [1] Abel, T., Norman, M.L., & Madau, P., 1999, ApJ, 523, 66
- [2] Bernstein, J., 1988, Kinetic theory in the expanding universe, Cambridge
- [3] Carrillo, J.A., Gamba, I.M., Majorana, A. & Shu, C.-W., 2003, J. Comp. Phys., 184, 498
- [4] Carrillo, J.A., Gamba, I.M., Majorana, A. & Shu, C.-W., 2006, J. Comp. Phys. (to appear)
- [5] Cen, R.Y., 2002, ApJ, 141, 211
- [6] Cen, R. & Haiman, Z., 2000, ApJL, 542, L75
- [7] Ciardi, B., Ferrara, A., Marri, M. & Raimondo, G., 2001, MNRAS, 324, 381
- [8] Feng, L.L., Shu, C.-W., & Zhang, M.P., 2004, ApJ, 612, 1
- [9] Gnedin, N.Y. & Abel, T., 2001, NewA, 6, 437
- [10] Jiang, G. & Shu, C.-W., 1996, J. Comp. Phys., 126, 202
- [11] Madau, P. & Rees, M., 2000, ApJL, 542, L69
- [12] Maselli, A., Ferrara, A., & Ciardi, B., 2003, MNRAS, 345, 379
- [13] Osterbrock, D., 1989, Astrophysics of Gaseous Nebulae and Active galactic Nuclei, University Science Books, California
- [14] Razoumov, A.O., Norman, M.L., Abel, T., & Scott, D., 2002, ApJ, 572, 695
- [15] Sokasian, A., Abel, T., & Hernquist, L.E., 2001, NewA., 6, 359
- [16] Spitzer, L., 1978, Physical Processes in the Interstellar Medium, John Wiley & Sons, NY
- [17] Strömgren, B., 1939, ApJ, 89, 529
- [18] Stuart, J., Wyithe, B., & Loeb, A., 2004, Nature, 427, 815
- [19] Theuns, T., Leonard, A., Efstathiou, G., Pearce, F.R. & Thomas, P.A., 1998, MNRAS, 301, 478
- [20] White, R.L., Becker, R.H., Fan, X.H. & Strauss, M., 2003, ApJ, 126, 1
- [21] Xu, Z. & Shu, C.-W., 2005, J. Comp. Phys., 205, 458
- [22] Yu, Q.J., & Lu, Y.J., 2005, ApJ, 621, 31